Critical fields, Pauli paramagnetic limiting, and material parameters of Nb_3Sn and V_3Si

T. P. Orlando
Department of Physics, Stanford University, Stanford, California 94305

E. J. McNiff, Jr. and S. Foner
Francis Bitter National Laboratory, Massachusetts Institute of Technology, Cambridge, Massachusetts 02139

M. R. Beasley
Department of Applied Physics and Electrical Engineering, Stanford University, Stanford, California 94305

(Received 9 November 1978)

The upper-critical-field behavior of Nb_3Sn and V_3Si is studied as a function of residual resistivity. The results are analyzed in the framework of the Ginzburg-Landau-Abrikosov-Gor'kov theory of type-II superconductivity including the effects of the electron-phonon interaction. The importance of the electron-phonon interaction on the Pauli paramagnetic limiting process is stressed and it is found that inclusion of the electron-phonon corrections (most importantly the electron-phonon renormalization of the normal-state parameters) is needed to sensibly fit the data. For Nb_3Sn failure to include these effects leads to too high spin-orbit scattering rates. The critical-field data are also used to determine the density of states of these materials as well as several other superconducting and normal-state parameters.

I. INTRODUCTION

The A-15 superconductors are of continuing interest both scientifically and practically. In this paper we report a study of the upper critical field $H_{c2}(T)$ of Nb_3Sn and V_3Si on a series of dual-electron-beam-coevaporated thin films with differing residual resistivities. Because these films are well characterized (including superconducting tunneling measurements on the same or similar films) it has been possible to analyze the data in detail. We have compared our results at both low and high fields with the predictions of the Ginzburg-Landau-Abrikosov-Gor'kov (GLAG) theory of type-II superconductivity including corrections for the electron-phonon interaction.

A surprising conclusion of this study is that the apparent absence of Pauli paramagnetic limiting in Nb_3Sn (i.e., the apparent absence of any reduction of H_{c2} below that value expected on the basis of orbital pair-breaking alone) and by contrast its presence in V_3Si results significantly from the stronger electron-phonon interaction in Nb_3Sn compared with V_3Si. In the past the apparent absence of Pauli limiting in Nb_3Sn has been attributed to only a spin-orbit scattering rate. Simple physical arguments show that the electron-phonon interaction increases the Pauli limiting field above its BCS value. As a result, less spin-orbit scattering is needed to account for the observed behavior. An analysis of the data without corrections for the electron-phonon interaction leads to unrealistically large spin-orbit scattering rates for Nb_3Sn. Since the corrections arise primarily from the electron-phonon renormalizations of normal-state parameters, and only secondarily from the strong-coupling corrections to the superconductivity, they are non-negligible even in relatively-weak-coupled superconductors. This fact appears not to have been appreciated previously. Electron-electron interactions can also affect (decrease) the Pauli limiting field. The implications of these further corrections on our results are also discussed.

Using the GLAG relationships and our measured critical-field slopes near T_c, we also calculate the coefficient of the electronic heat capacity γ and the related electronic density of states $N(0)$ as a function of residual resistivity. Our results agree with those obtained directly from heat-capacity measurements. From our data we also generate a self-consistent set of superconducting and normal-state material parameters [e.g., $\xi_{GL}(0)$, $\lambda_{GL}(0)$, ξ_0, l_{tr}, $N(0)$ and v_F] for these two materials.

On the more practical side, our results for Nb_3Sn suggest that with proper treatment (i.e., moderately increasing the resistivity) the critical field at zero temperature $H_{c2}(0)$ can be raised significantly (to $\simeq 300$ kOe) at the expense of only a slight decrease

in T_c. At the other extreme our results imply that very clean Nb_3Sn should have a critical field at zero temperature of $\simeq 210$ kOe.

This paper is organized as follows. In Sec. II the experimental procedures are outlined. The data are presented in Sec. III along with a discussion of the effects of the electron-phonon interaction on the critical fields and an interpretation of the data. The material parameters derived from the critical-field measurements are also presented in Sec. III. Section IV summarizes the results and their implications.

II. EXPERIMENTAL PROCEDURE

A. Sample preparation

In this study a set of samples with fixed composition but varying residual resistivities ρ were desired. The samples were prepared as thin films ($\simeq 0.3\mu$m thick) by electron-beam coevaporation onto $\frac{1}{4}$-in. square sapphire substrates using the techniques of Hammond.[1] These techniques are now highly developed, providing high-quality A-15 films and allowing considerable control over the material properties.[2] As shown by Moore, *et al.*,[3] at Stanford in their tunneling studies, the best quality Nb_3Sn and V_3Si thin films (highest T_c's and resistance ratios RR) are obtained for "hot" and "slow" depositions, specifically depositions at a substrate temperature $T_s \simeq 850\,^{\circ}$C and at a deposition rate $\lesssim 3$ nm/sec. Moreover such films are found to grow as columnar grains preferentially oriented along a [100] direction. Higher resistivity films (with correspondingly reduced T_c's) were obtained by depositing at lower substrate temperatures.

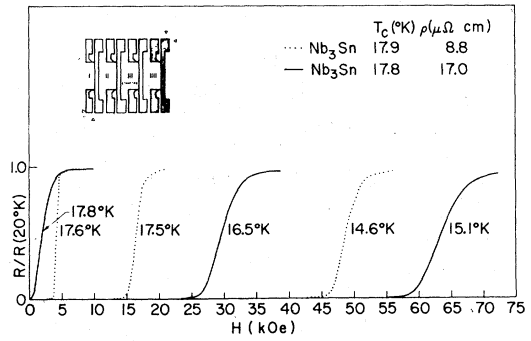

FIG. 1. Resistive transitions of Nb_3Sn thin films using field sweeps at constant temperatures. The sample (dotted line) with the lower residual resistivity has the sharpest transition. The other Nb_3Sn sample (solid line) with a higher residual resistivity has a wider transition, which is representative also of the V_3Si thin films. Note that the width of the transition tends to broaden in higher fields. The insert shows the photolithographed pattern of the thin-film samples.

To facilitate the resistivity and critical-field measurements most of the films were photolithographed and etched to the pattern shown in the insert of Fig. 1. With such patterned samples the resistivity and superconducting resistive transitions could be obtained with a four-point resistance measurement. For the unpatterned samples the resistivity was measured using the Van der Pauw method.[4] Also, since the samples were deposited in a compositional "phase-spread" configuration, the unpatterned samples vary to some degree in composition across the films. Table I lists the samples studied along with the deposition temperature (T_s) and other physical properties (T_c, ρ, dH_{c2}/dT) of interest. The composition is denoted by $\%B$, the atomic percent of the B element in the nominal compounds A_3B, and has been measured to an accuracy of $\pm 1.5\%$ by electron microprobe analysis. The thickness d of the films was measured by the Tolansky method.

B. Critical-field measurements

The critical fields were determined from both ac and dc resistive transitions. Some typical traces using a field sweep at constant temperature are shown in Fig. 1. All samples were measured in low fields (near T_c) using a 105-kOe (at ~ 2.2 K) Nb-Ti superconducting magnet at Stanford. Selected samples were also measured up to ~ 230 kOe using the facilities of the Francis Bitter National Laboratory.

As seen in Fig. 1 the best Nb_3Sn sample ($\rho(20\text{ K}) = 8.8\mu\Omega$ cm, RR [$= \rho(300\text{ K})/\rho(20\text{ K})$] of 9.5) has a very narrow transition. The other Nb_3Sn films and the V_3Si films have broader transitions. The behavior of the Nb_3Sn sample with $\rho = 17\mu\Omega$ cm shown in Fig. 1 is representative of these other samples. The transitions of all samples tend to broaden in high fields, which may introduce some systematic errors. However, even if the 10% or 90% points of the transition curves are taken to define $H_{c2}(T)$, the reduced field,

$$h \equiv \frac{H_{c2}}{(dH_{c2}/dT)_{T_c} T_c}$$

and the reduced temperature, $t = T/T_c$, are the same at temperatures near T_c.

As a complement to sweeping the field, in some measurements the temperature was swept in a fixed field; here the midpoint of the transitions reproduced the same phase boundary, $H_{c2}(T)$. In addition to the resistive transitions, the opening of the superconducting energy gap was also used to measure $H_{c2}(T)$ on some samples upon which good tunnel junctions had been made; these measurements also reproduced the same phase boundary.

TABLE I. Properties of samples studied.

	T_c (°K)	$\frac{dH_{c2}}{dT}\|_{T_c}$ (kOe/K)	ρ_{T_c}[a] ($\mu\Omega$ cm)	%B (at.%)	d (μm)	T_s (°C)
			Nb_3Sn			
76 – 26 – 7A[b]	17.9	19.4	16.0	27.9	0.21	850
76 – 28 – 7B	17.9	18.3	8.8	26.9	0.73	850
76 – 25 – 6B	17.8	22.1	17.0	27.1	0.26	850
G – 77 – 34 – 6C – III	16.1	25.5	35.9	26.2	0.51	710
			V_3Si			
76 – 97 – 4B	16.4	18.4	5.2	26.0	1.0	875
77 – 4 – 5C	16.1	19.0	7.2	24.6	0.30	875
76 – 92 – 8A	15.7	20.3	15.1	25.9	0.30	750
77 – 4 – 6B	15.6	17.8	6.1	25.8	0.30	875
76 – 93 – 5C	14.8	22.7	31.2	26.1	0.30	650
76 – 93 – 6C – II	14.3	22.4	37.9	27.4	0.30	650
76 – 93 – 6C – III	13.9	23.1	39.5	27.4	0.30	650
77 – 4 – 2A – II	13.8	· · ·	42.6	21.2	0.30	875
76 – 96 – 4C	13.6	26.5	43.2	23.6	0.30	550
77 – 4 – 2A – III	12.9	30.4	42.6	21.2	0.30	875

[a]The resistivity just above T_c is denoted here by ρ_{T_c} and in the text by ρ.

[b]Sample designation gives year, deposition number, and sample number in sequence and can be used to cross-reference data on samples in other references (e.g., Ref. 3 and Ref. 24 of this paper).

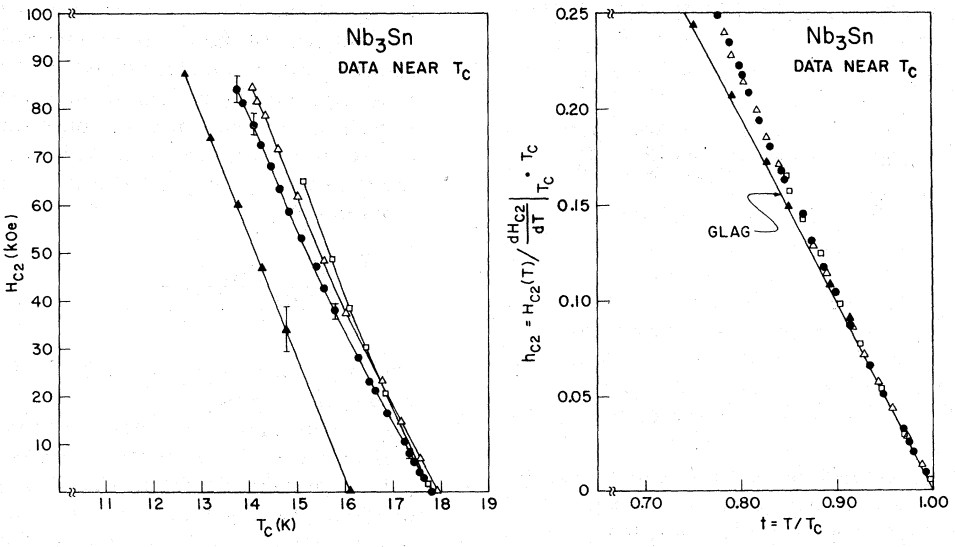

FIG. 2. Low-field critical fields of Nb_3Sn with various residual resistivities plotted in both applied and reduced variables. The samples show a progression from higher to lower T_c and lower to higher $(dH_{c2}/dT)_{T_c}$ as the sample residual resistivity is increased. (See Table I.) The "clean" samples (□, Δ, ●), curve positively from the theoretical GLAG curve. The "dirty" sample (Δ) with higher residual resistivity and lower T_c lies on the theoretical GLAG curve.

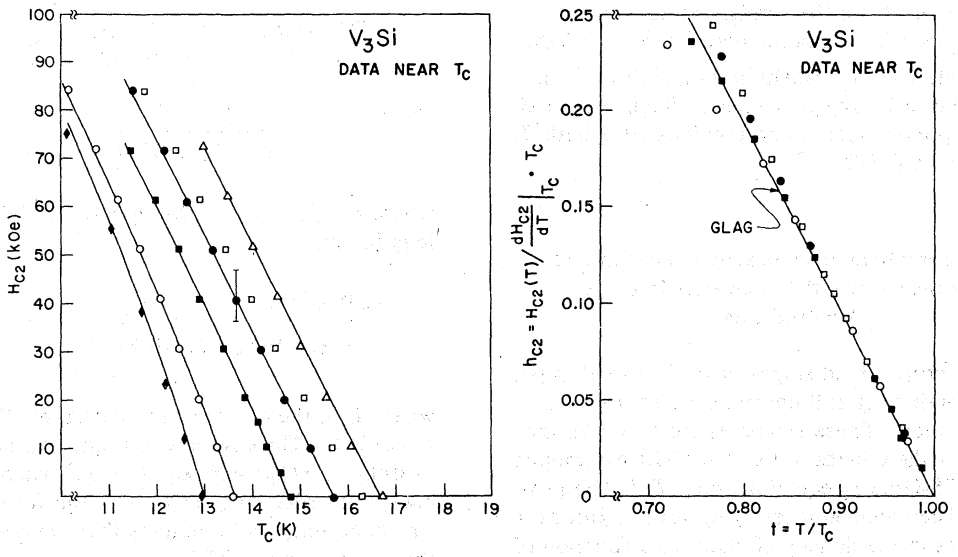

FIG. 3. Low-field critical fields of V_3Si with various residual resistivities plotted in both applied and reduced variables. Like Nb_3Sn the samples show a progression from higher to lower T_c and lower to higher $(dH_{c2}/dT)_{T_c}$ as the residual resistivity is increased. (See Table I).

III. CRITICAL-FIELD DATA

A. Low-field data near T_c

In general, the samples deposited on a hot substrate have the lowest residual resistivities, the highest transition temperatures, the sharpest transitions, and the lowest critical-field slopes. The critical-field curves near T_c for the Nb_3Sn and the V_3Si samples are shown in Figs. 2 and 3, respectively. For V_3Si a wider range of transition temperatures was observed. The data in Fig. 3 are representative, and the critical field slopes on additional samples are listed in Table I.

The data for Nb_3Sn show that the $H_{c2}(T)$ phase boundary for the three cleaner samples ($T_s = 850$ C) with $T_c \simeq 17.8$ K, all curve positively from the straight line expected near T_c from the GLAG theory.[5] (As will be shown in Fig. 7, positive curvature is also present in the single crystal data for the nominally tetragonal phase of Nb_3Sn obtained earlier by two of us).[6] In contrast, the dirtier sample ($T_s = 710$ C) with $T_c = 16.3$ K shows no such curvature and lies precisely on the theoretical GLAG curve for orbital pair breaking. As can be seen in the reduced field and temperature plots in Fig. 3, the cleanest V_3Si with a high T_c and a low $(dH_{c2}/dT)_{T_c}$ also has positive curvature, but much less than Nb_3Sn. The dirtiest V_3Si with a low T_c and a high $(dH_{c2}/dT)_{T_c}$, on the other hand, falls below the GLAG curve for orbital pair breaking, indicative of Pauli limiting.

The dependence of T_c and $(dH_{c2}/dT)_{T_c}$ on ρ is

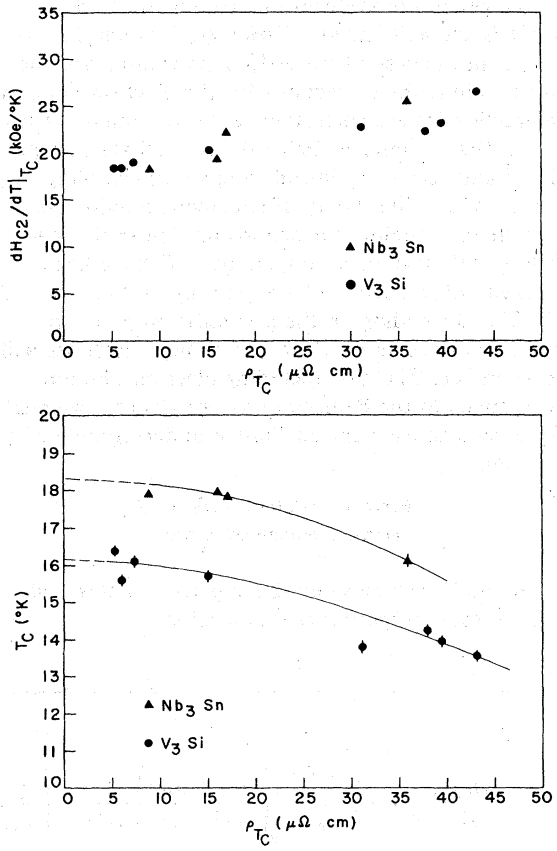

FIG. 4. Variation of the critical-field slopes and critical temperatures of Nb_3Sn and V_3Si as a function of residual resistivity (above T_c). For both materials, as the resistivity increases, the critical-field slope increases and the transition temperature decreases.

shown in Fig. 4. Note the similar increases in $(dH_{c2}/dT)_{T_c}$ as ρ increases for both Nb_3Sn and V_3Si. For both materials the transition temperature T_c decreases as the resistivity ρ increases. Such systematic trends with ρ have been noted previously for both T_c (Ref. 7) and $(dH_{c2}/dT)_{T_c}$.[8]

B. Determination of some superconducting and normal-state material parameters from the low-field data

From the critical-field slopes near T_c several important superconducting and normal-state parameters can be estimated. These estimates are based on the evaluation of the Ginzburg-Landau (GL) parameters from the BCS-Gorkov equations near T_c.[9] The procedure has been applied recently by several groups to infer changes in the density of states as a function of disorder.[8] We carry out a similar but more complete analysis here. Also, for V_3Si, heat-capacity measurements are available on a disordered sample with which we compare our results directly.[10]

The general procedures involved in such an analysis are well known. However, for quantitative results in the case of the A-15 superconductors one must include the corrections for the electron-phonon interaction. These corrections enter the theory in two ways: first by renormalizing the normal-state properties,[11] and second by introducing strong-coupling corrections to the theory of superconductivity itself. The strong-coupling corrections needed in the low-field Ginzburg-Landau regime near T_c have been worked out in detail and are typically on the order of 10–20% depending on the particular property and material in question. However, at high fields we will show in Sec. III C that including electron-phonon corrections to the Pauli-limiting process are essential for even a satisfactory qualitative understanding of the data.

Theoretical relations—effects of electron-phonon interaction

The main link between the superconducting and normal-state properties that is used is

$$-\frac{dH_{c2}}{dT}\Big|_{T_c}^{\rm BCS}=\frac{24\pi^2}{7\zeta(3)}\frac{k_B^2c}{\hbar e}\frac{T_c}{v_F^2}\chi^{-1}(\lambda_{\rm tr}) \tag{1}$$

$$\equiv\frac{\hbar c}{2e}\frac{1}{\xi_{\rm GL}^2(0)}\frac{1}{T_c}\ , \tag{2}$$

where $\xi_{\rm GL}(0)$ is the zero-temperature GL coherence length, and

$$\lambda_{\rm tr}\equiv\hbar/2\pi k_BT_c\tau_{\rm tr}$$
$$=\hbar v_F/2\pi k_BT_cl_{\rm tr}=0.9\xi_0/l_{\rm tr}\ ,$$

where $l_{\rm tr}$ is the transport scattering length. Here $\chi(\lambda_{\rm tr})$ is the Gorkov function, and can be expressed usefully as $\chi(\lambda_{\rm tr})=R(\lambda_{\rm tr})/(1+\lambda_{\rm tr})$ where $R(\lambda_{\rm tr})$ is always of order unity [$R(0)=1$ and $R(\infty)=1.17$].[9] The superscript BCS denotes that the result applies in the weak-coupling BCS limit.

The corrections to the Ginzburg-Landau parameters due to a strong electron-phonon interaction have been studied by various authors.[12–20] The most important result for our purposes is that the slope of the upper critical field near T_c can be written

$$\frac{dH_{c2}}{dT}\Big|_{T_c}=\eta_{H_{c2}}(T_c)\frac{dH_{c2}(x^*)}{dT}\Big|_{T_c}^{\rm BCS}\ , \tag{3}$$

where x^* denotes that in calculating $(dH_{c2}/dT)_{T_c}$ one must use renormalized normal-state parameters [e.g., $v_F\rightarrow v_F^*=v_F^b/(1+\lambda_{ep})$] in the weak-coupled BCS expressions. Here λ_{ep} is the usual electron-phonon interaction parameter

$$\lambda_{ep}=2\int_0^\infty\alpha^2(\omega)F(\omega)\omega^{-1}\,d\omega$$

and the superscript b refers to band values. The parameter $\eta_{H_{c2}}(T_c)$ is the ratio of the strong-coupled magnetic pair-breaking parameter to the weak-coupled BCS value, and can be calculated if the electron-phonon spectral function $\alpha^2F(\omega)$ is known.[13–17] Similar relationships hold for other superconducting properties (e.g., H_c, $2\Delta/kT_c$). Also the equation for $(dH_{c2}/dT)_{T_c}$ can be written[12]

$$-\frac{dH_{c2}}{dT}\Big|_{T_c}=\frac{\eta_{H_{c2}}(T_c)}{R(\lambda_{\rm tr})}\left[\left(\frac{24\pi^2}{7\zeta(3)}\frac{k_B^2c}{\hbar e}\right)\frac{T_c}{v_F{}^{*2}}+\left(\frac{12\pi}{7\zeta(3)}\frac{k_Bc}{e}\right)\frac{1}{v_F{}^*l}\right] \tag{4}$$

$$=\eta_{H_{c2}}(T_c)\frac{R(\infty)}{R(\lambda_{\rm tr})}\left[1.18\times10^{29}\frac{T_c^2\gamma^*}{S^2}+4.40\times10^4\rho\gamma^*\right]\ , \tag{5}$$

where γ^* is the renormalized electronic heat-capacity coefficient, ρ is the resistivity, and S is the Fermi-surface area.

Several comments regarding Eqs. (4) and (5) are in order. First, we have placed asterisks only on those normal-state parameters actually renormalized by the electron-phonon interaction. (See Ref. 11 for a summary.) Second, in going from Eq. (4) to Eq. (5), we have assumed a spherical Fermi surface so that we have

$$\langle v_F^* \rangle \geq \langle 1/v_F^* \rangle^{-1} = k_B^2 S (6\hbar\gamma^*)^{-1} \tag{6}$$

and

$$l_{tr} = 6\pi^2 \hbar (e^2 S \rho)^{-1} (9 \times 10^{11}) \ . \tag{7}$$

The formula for l_{tr} is valid only for cubic or isotropic systems. Nevertheless, we have found that these formulas work well in spite of the simplifying assumptions. Finally, in Eqs. (5)–(7) the units of dH_{c2}/dT are given in Oe/K, ρ in Ω cm, and γ^* in erg/cm^{3}K^2.

From Eq. (4), once $\eta_{H_{c2}}$ is known, measurements of T_c, $(dH_{c2}/dT)_{T_c}$ and ρ provide information about the average Fermi velocity of the material. [Of course the GL coherence length $\xi_{GL}(0)$ follows directly from Eq. (2).] What is more useful here, however, is to assume that Eqs. (6) and (7) are valid and use Eq. (5) along with measurements of T_c, $(dH_{c2}/dT)_{T_c}$ and ρ to calculate the coefficient of the electronic heat capacity γ^*, which is currently of considerable interest for the A-15 materials. In the dirty limit ($\lambda_{tr} \approx 1.2\xi_0/l_{tr} >> 1$) the second term in Eq. (5) dominates and this procedure is unambiguous. In the clean limit ($\lambda_{tr} << 1$) the value of the Fermi surface area S is needed to determine γ^*.

2. Determination of the parameters

In principle to obtain $\eta_{H_{c2}}$ and carry out the above scheme, $\alpha^2F(\omega)$ is needed. Fortunately, the various strong coupling corrections are not sensitive to the detail shape of $\alpha^2F(\omega)$ and can be estimated with relationships obtained from simple Einstein or Debye models. Several such methods for estimating λ_{ep} and the η's exist in the literature.[12,13,18–20] We have done the following:

Using T_c and the measured values of $2\Delta/k_BT_c$ from the tunneling data on the same films, we calculated the equivalent Einstein frequency ω_0 from the analytical expression for $2\Delta/k_BT_c$ in terms of T_c/ω_0 obtained by Kresin and Parkhomenko[19] based on a simple Einstein spectrum for $\alpha^2(\omega)F(\omega)$. The η's and λ_{ep} then followed from T_c and ω_0.[19–20] (See Appendix A1.) Table II lists these parameters for our cleanest Nb_3Sn and V_3Si.

The γ^* inferred from our measurements and from data using the procedure outlined above (See Appendix 2) are shown in Figs. 5 and 6. For comparison the γ^*'s obtained from heat capacity measurements are also shown.[10,21,22] The error bars show the sensitivity of γ^* to the assumed area of the Fermi surface S which has been listed as a fraction of S_F, the Fermi surface of a free-electron gas density n. (See Reference 23.) For the reasons mentioned above, this uncertainty is only important in the clean limit.

The correspondence between the thermal and magnetic measurements is satisfactory, given the uncertainties. The results for V_3Si are particularly important since the thermal data compare well with the magnetic data in both the clean and dirty limits, even though the resistivities were induced by neutron irradiation in the case of the thermal data and induced by low deposition temperatures in the case of the magnetic data. Thus the low-field critical-field data of these A-15 superconductors are in good agreement with the GLAG theory. Moreover, the agreement between thermally versus magnetically derived γ^*'s implies that *there is no dramatic difference between the density of states governing thermal and electronic transport properties in these materials.* This in turn justifies the use of critical-field measurements to study systematic changes in the density of states of the A-15 superconductors when heat-capacity measurements are not available.

With a more complete set of relationships (See Appendix) it is possible to infer additional important material parameters for Nb_3Sn and V_3Si. These are

TABLE II. Strong-coupling parameters for Nb_3Sn and V_3Si.

	T_c (K)	$\frac{2\Delta_0}{k_BT_c}$	ω_0 (meV)	λ_{ep}	μ^*	$\eta_{Hc}(0)$	$\eta_{H_{c2}}(T_c)$
Nb_3Sn	17.8	4.2	11.4	1.8	0.10	1.42	1.17
V_3Si	16.4	3.7	24	0.96	0.10	1.11	1.05

Note the underlined quantities were measured; the others inferred, with μ^* taken to be 0.1.

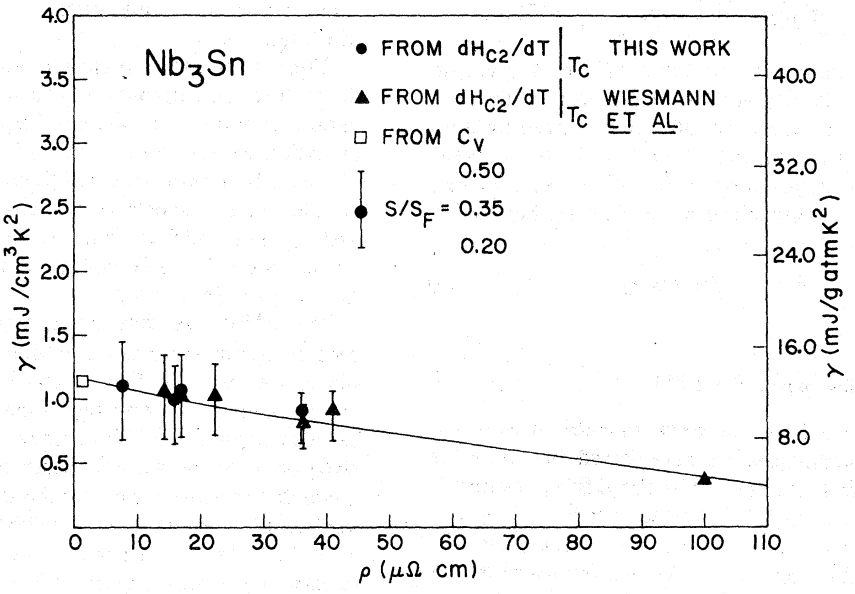

FIG. 5. The coefficient of the electronic heat capacity, γ, inferred from $H_{c2}(T)$ measurements and thermal measurements of Nb_3Sn samples with different residual resistivities (above T_c). Note the consistency of thermal (Refs. 21 and 22) and magnetic data. In the case of the data by Weismann *et al.* (Ref. 8) the resistivity was increased by α-particle irradiation.

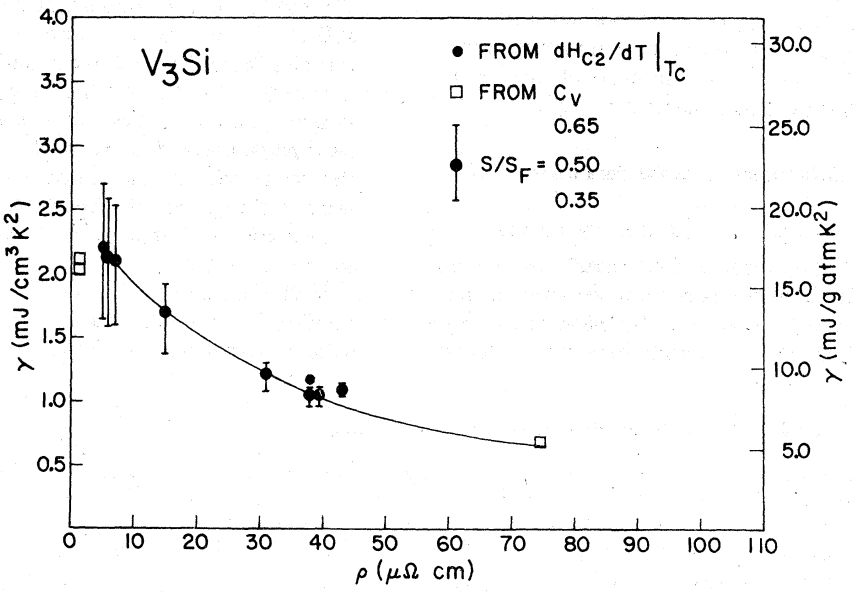

FIG. 6. The coefficient of the electronic heat capacity, γ, inferred from $H_{c2}(T)$ measurements and thermal measurements for V_3Si samples with different residual resistivities (above T_c). Like Nb_3Sn, note the consistency between thermal and magnetic data. In the case of the thermal data for the high-resistivity sample (Ref. 10) the resistivity was increased by means of neutron irradiation.

given in Table III. The uncertainties show the effect of varying the Fermi-surface area S. The mean values correspond to choosing S so as to make the γ^*'s determined thermally and from $(dH_{c2}/dT)_{T_c}$ agree for the cleanest sample. For the other samples, S is fixed at this value. An independent check of this procedure for determining S is available for Nb_3Sn. From the results in Table III we have estimated the zero-temperature penetration depth $\lambda(0)$ for Nb_3Sn to be 1000 Å which agrees well with 1300 Å measured recently by Howard, Rudman and Beasley using Josephson tunneling on similar films.[24] More extensive measurements of λ, particularly near T_c, would allow the complete set of material parameters shown in Table III to be established unambiguously.

C. High-field data and comparison with theory

The high-field behavior of our samples is shown in Figs. 7 and 8, for both applied field and temperature and also the reduced variables h and t. For both materials, single crystal data[6] are also shown for comparison.

For Nb_3Sn the single crystal data (H along the [100] direction) are essentially identical to that found for our cleanest thin films (also preferentially oriented along the [100] direction), including the curvature near T_c. Also evident in Fig. 7 is that for the dirtier Nb_3Sn, $H_{c2}(0)$ is larger than for the cleaner material, reflecting the higher $(dH_{c2}/dT)_{T_c}$ and only slightly reduced T_c. By contrast, for V_3Si the cleanest film is qualitatively but not quantitatively similar to the single-crystal data. This suggests our best V_3Si films are still short of ideal. Moreover, our dirtier films do not show an enhanced $H_{c2}(0)$ relative to the cleaner samples to any substantial degree even though $(dH_{c2}/dT)_{T_c}$ T_c is larger. This result is associated with the existence of strong Pauli limiting in V_3Si as compared with Nb_3Sn discussed in considerable detail below.

1. *Qualitative aspects of the data*

Although the low-field behavior of Nb_3Sn and V_3Si are very similar, the high-field data are strikingly different. Nb_3Sn shows no apparent signs of Pauli limiting whereas V_3Si shows substantial Pauli limiting. More explicitly, in Fig. 7 the theoretical curves shown correspond to the predictions of the GLAG theory, including only orbital pair-breaking, in the clean and dirty limit fitted to the measured T_c and critical-field slopes of our Nb_3Sn samples.

As seen in Fig. 7, the higher resistivity, lower-T_c

TABLE III. Some important superconducting and normal-state material parameters of Nb_3Sn and V_3Si.

	ρ (20 K) ($\mu\Omega$ cm)	T_c (K)	γ^* $\left(\frac{\text{mJ}}{\text{cm}^3 K^2}\right)$	$N^*(0)$ $\left(\frac{\text{states}}{\text{ev spin unit cell}}\right)$	$N^b(0)$ $\left(\frac{\text{states}}{\text{eV spin unit cell}}\right)$	V_F^* $\left(10^7 \frac{\text{cm}}{\text{sec}}\right)$	V_F^b $\left(10^7 \frac{\text{cm}}{\text{sec}}\right)$	λ_{ep}	S/S_F	ξ_0^* (nm)	l_{tr} (nm)	$\xi_{GL}(0)$ (nm)	$\lambda_{GL}(0)$ (nm)
Nb_3Sn (low resistivity) $76-28-7B$	8.8	17.9	1.1 ±0.4	21 ±8	7.5 ±3	0.74 ±0.06	2.1 ±0.2	1.78	0.35 ±0.15	5.7 ±0.5	10 ∓4	3.2	64 ∓7
Nb_3Sn (high resistivity) $G-77-34-6C-III$	35.9	16.1	0.91 ±0.15	17 ±3	6.6 ±1.2	0.90 ±0.15	2.3 ±0.4	1.6	0.35 ±0.15	7.7 ±1	2.6 ∓1	2.8	93 ∓14
V_3Si (low resistivity) $76-97-4B$	5.2	16.4	2.2 ±0.2	30 ±7	15 ±3.5	0.67 ±0.03	1.31 ±0.06	0.96	0.50 ±0.15	5.6 ±0.3	9.5 ∓2	3.3	62 ∓7
V_3Si (high resistivity) $76-96-4C$	43.2	13.6	1.1 ±0.2	15.2 ±0.2	8.2 ±0.1	1.2 ±0.3	2.3 ±0.6	0.86	0.50 ±0.15	13 ±3	1.2 ∓0.4	3.0	114 ∓3

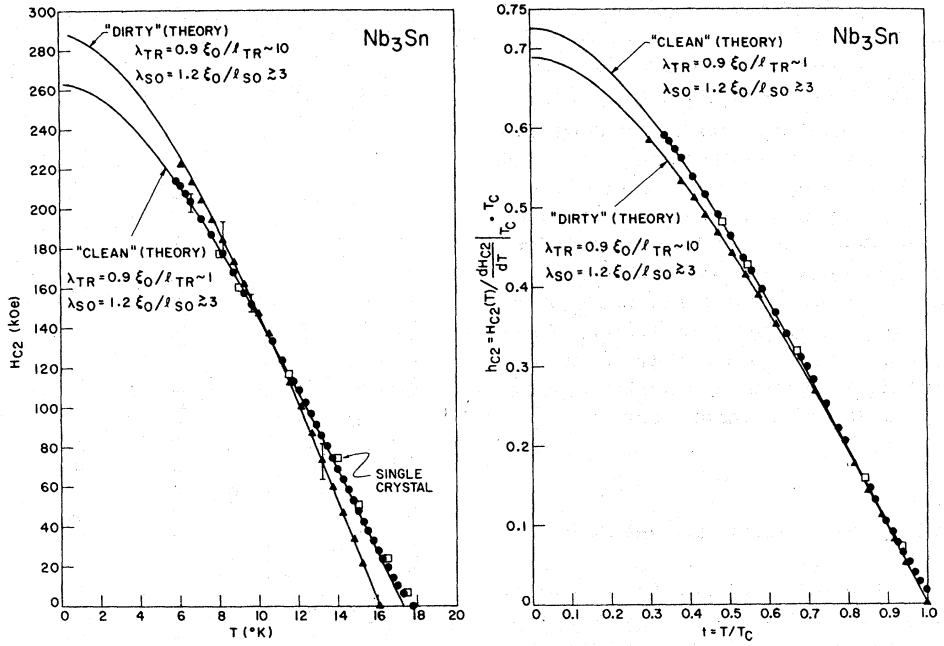

FIG. 7. Critical fields of Nb_3Sn with different residual resistivities plotted in both applied and reduced variables. The critical field of "clean" thin film (•) agrees well with that of the nominally tetragonal phase (□) of Ref. 6. The "dirty" thin film (Δ) has a lower T_c but a higher $(dH_{c2}/dT)_{T_c}$ so that it extrapolates to a higher $H_{c2}(0)$ than the "clean" thin film. None of the samples show any Pauli paramagnetic limiting within experimental error. The theoretical curves shown are for the GLAG theory assuming only orbital pair breaking. The minimum spin-orbit scattering parameters λ_{so} (including the electron-phonon interaction corrections discussed in the text) consistent with this apparent absence of Pauli limiting are also shown in the figure.

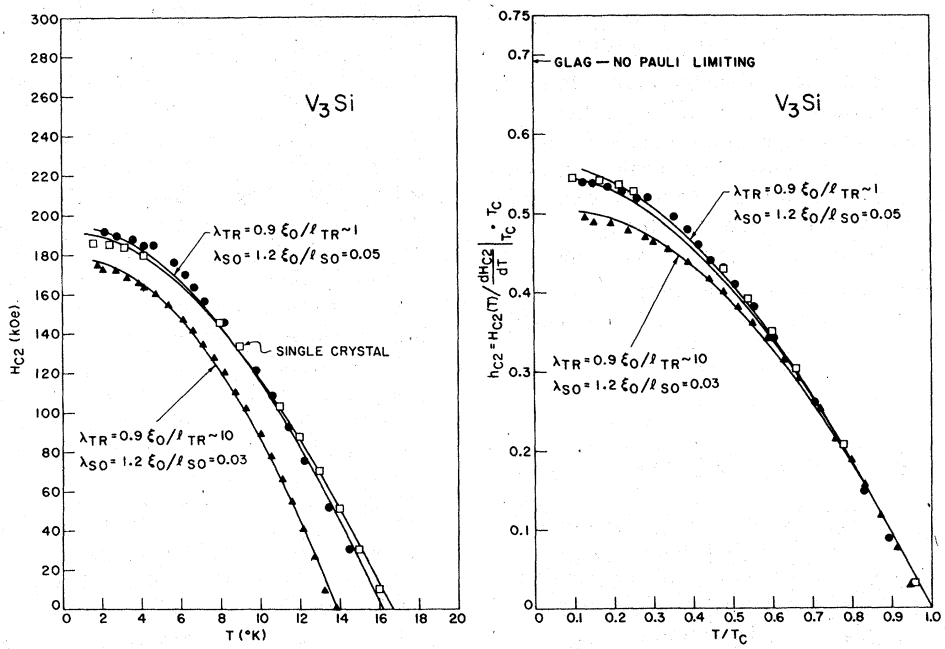

FIG. 8. Critical fields of V_3Si with different residual resistivities plotted in both applied and reduced variables. The critical field of the thin film with the higher T_c (•) agrees qualitatively with that of the single crystal of Ref. 6. All of the V_3Si are strongly Pauli paramagnetically limited. The theoretical curves shown are for the GLAG theory including both orbital and Pauli pair breaking *and* the electron-phonon interaction corrections as discussed in the text. The spin-orbit scattering parameters are shown in the figure along with the transport scattering parameters.

film of Nb_3Sn is fitted well with the dirty limit curve. This is consistent with our estimate $\lambda_{tr} \sim 10$ for that sample. The data for the lower resistivity high-T_c thin-film and single-crystal Nb_3Sn both have positive curvature near T_c, and one must decide whether to fit the curves with the measured slope of $(dH_{c2}/dT)_{T_c}$, and the measured T_c or whether to seek the best overall fit which in effect uses an averaged slope in the region from 20 kOe to 100 kOe and an extrapolated transition temperature.[6] With the former procedure the data lie higher than the theoretical maximum of the clean limit curve. Using the latter (shown in the figure) the data follow very well the clean limit curve from 20 kOe upwards. Such clean behavior is consistent with the estimate $\lambda_{tr} \simeq 1$ for this sample. In any event there is no evidence for Pauli limiting. V_3Si on the other hand falls well below the GLAG predictions assuming no Pauli limiting as seen in Fig. 8b. The theoretical fits to the V_3Si data and the procedures used to estimate the values of the spin-orbit scattering parameters λ_{so} shown on the figures are discussed in Sec. III C.2.

2. Quantitative comparison with theory—Pauli paramagnetic limiting and the effects of the electron-phonon interaction

Before comparing our results quantitatively with theory,[25–27] it is necessary to discuss how the electron-phonon coupling affects the GLAG theory at high fields. In the absence of Pauli limiting the strong-coupling corrections can be written

$$H_{c2}(T) = \eta_{H_{c2}}(T) H_{c2}^{\mathrm{BCS}}(x^*) \tag{8}$$

or

$$h_{c2}(t) = \eta_{h_{c2}}(t) h_{c2}^{BCS}(x^*) \ . \tag{9}$$

A strong-coupling theory of H_{c2} including Pauli limiting has been worked out by D. Rainer, G. Bergmann, and U. Eckhardt[14] but not accompanied by a simple physical interpretation nor in a form suitable for evaluation without complete knowledge of $\alpha^2F(\omega)$. However, physical insight into how the electron-phonon interaction affects Pauli limiting and an approximate framework for analyzing the data can be obtained as follows. Consider first the simple Pauli limiting field H_p (i.e., with no other pair breaker and in the absence of spin-orbit scattering). From the thermodynamic definition of H_p as that field at which the free energy of the normal state with spin susceptibility χ_n equals the condensation energy of the superconductor we have at zero temperature

$$\tfrac{1}{2}\chi_n H_p^2(0) \equiv \frac{1}{8\pi} H_c^2(0)$$

$$= \frac{1}{8\pi}\eta_{H_c}^2(0)[H_c^{\mathrm{BCS}}(x^*)]^2 \tag{10}$$

$$= \tfrac{1}{2}\eta_{H_c}^2 N^*(0)(1.78 k_B T_c)^2 \ , \tag{11}$$

where η_{H_c} is the strong-coupling superconducting correction to H_c and $N^*(0) = (1+\lambda_{ep})N^b(0)$ is the density of states renormalized by the electron-phonon interaction. To calculate H_p we note that the spin susceptibility is determined by the band density of states

$$\chi_n = 2\mu_B^2 N^b(0)$$

and, thus at $T=0$, we have

$$H_p(0) = \eta_{H_c}(0)(1+\lambda_{ep})^{1/2}\frac{1.78 k_B T_c}{2^{1/2}\mu_B} \tag{12}$$

$$= \eta_{H_c}(0)(1+\lambda_{ep})^{1/2} 18.6 T_c \ (\mathrm{kOe}) \ , \tag{13}$$

which is a factor of $\eta_{H_c}(0)(1+\lambda_{ep})^{1/2}$ larger than the usual BCS value. Note that even in the case of a weak-coupled superconductor for which $\eta_{H_c}(0)=1$, the correction factor $(1+\lambda_{ep})^{1/2}$ remains as a consequence of the different electron-phonon renormalizations of the density of states that enter H_c and χ_n. The existence of this factor was recognized in the original paper on Pauli paramagnetic limiting by Clogston,[28] but has apparently never been properly included in quantitative studies of Pauli limiting. Even in the case of Al — the canonical weak-coupled superconductor — $\lambda_{ep} \simeq 0.4$, and thus $H_p(0)$ is larger than the BCS value by about 20%. Additional corrections for the electron-electron interactions (e.g., the Stoner factor) should be included in a complete theory of Pauli limiting.[29]

For a quantitative analysis of our data it is necessary to include pair breaking due to both orbital effects and Pauli limiting. To do this approximately, we have first assumed that $\eta_{H_{c2}}(T)$ is independent of temperature. It follows that $\eta_{h_{c2}}(t)=1$ and hence the shape of the usual h vs t plot is unaffected. This assumption should be well justified for V_3Si which is less strongly coupled. Based on the numerical calculation of $\eta_{H_{c2}}(t)$ for several very strong-coupled superconductors this assumption seems fairly reasonable.[13] [According to the calculations in Ref. 13, only materials with a large weight in $\alpha^2(\omega)F(\omega)$ at very low frequencies (e.g., amorphous materials) have an enhanced $\eta_{h_{c2}}(t)$.] Second, to include Pauli limiting

we have simply replaced $H_p(0)$ (more precisely the Pauli-limiting pair breaker) by the appropriate quantity scaled to include the factors $\eta_{H_c}(0)$ and $(1+\lambda_{ep})^{1/2}$ and have assumed the moderating effects of spin-orbit scattering enter the theory[25–27] in the usual way.[30]

Using this theoretical framework we have analyzed the high-field data shown in Figs. 7 and 8. As already mentioned before, neither "clean" nor "dirty" Nb_3Sn shows any Pauli limiting within experimental error even when strong-coupling effects are included. Assuming H_p is given by Eq. (12) (more precisely using a pair breaker suitably scaled) we can put a lower limit on the spin-orbit scattering parameters λ_{so}'s necessary to be consistent with our data. These values are shown in Fig. 7. However, if the BCS value for the Pauli field, $H_p(0)=18.6T_c$ (kOe) is used, the spin-orbit scattering rate needed to account for the observed absence of Pauli limiting is increased to an extent such that $\lambda_{so} >> \lambda_{tr}$, i.e., the inferred rate of spin-orbit scattering markedly *exceeds* the rate of transport scattering. The above inequality is physically unreasonable. With the electron-phonon interaction corrections included λ_{so} and λ_{tr} are roughly comparable. Thus we see that the strong-coupling corrections to the Pauli-limiting process are necessary to have a sensible fit to the data. The actual fitted parameters for these two cases are contrasted in Table IV for the clean Nb_3Sn sample for which the difference is most pronounced. The need to include the electron-phonon corrections is clear. Better quantitative work must await a much more detailed analysis (e.g., in Ref. 14), knowledge of $\alpha^2F(\omega)$, and possibly inclusion of electron-electron interactions.

Unlike Nb_3Sn, all the V_3Si samples show pronounced Pauli limiting. The fits to the data using the electron-phonon enhanced $H_p(0)$ are shown in Fig. 8. The fits obtained assuming the BCS value of $H_p(0)$ and the measured slopes and T_c's are less satisfactory as shown explicitly in Fig. 9. The data for V_3Si can be fitted in the high-field region with $H_p(0)=18.6T_c$ (kOe) but only by artificially increasing $(dH_{c2}/dT)_{T_c}$ and decreasing T_c to the values listed in Table IV. Thus, like Nb_3Sn, the critical-field behavior of V_3Si is better accounted for when the electron-phonon corrections to $H_p(0)$ are included. Moreover, our results imply that the absence of Pauli limiting in Nb_3Sn and its presence in V_3Si are related significantly to their relative degrees of electron-phonon coupling and that their spin-orbit scattering rates are lower than has been suggested before.

IV. DISCUSSION AND CONCLUSIONS

The data and analysis presented in the previous section show that the critical-field behavior of the *A*-15 superconductors Nb_3Sn and V_3Si are in general ac-

TABLE IV. Comparison of experimental parameters with fitted values.

		Measurement	fit with $H_p=\eta_{H_c}(0)(1+\lambda_{ep})^{1/2}18.6T_c$ (kOe)	fit with $H_p=18.6T_c$ (kOe)
Nb_3Sn	T_c (K)	17.3[a] (17.9)	17.3	17.3
	$(dH_{c2}/dT)_{T_c}$ (kOe/K)	20.5[a] (18.3)	20.5	20.5
	λ_{so}	. . .	>3	>10
	λ_{tr}	~1		
V_3Si	T_c (K)	16.1	16.2	15.5
	$(dH_{c2}/dT)_{T_c}$ (kOe/K)	20.0	22.0	27.5
	λ_{so}	. . .	0.05	0.25
	λ_{tr}	~1		

[a]The average slope from 20 kOe to 100 kOe and the extrapolated T_c are used here because of the positive curvature of H_{c2} near T_c as discussed in Sec. III C1. The slope and T_c at zero field are given in parentheses.

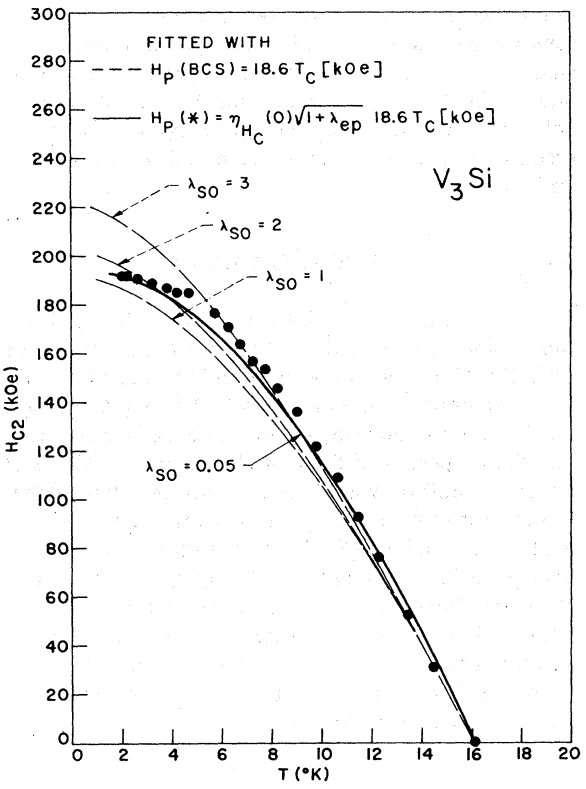

FIG. 9. Comparison of the theoretical fits to V_3Si with and without the corrections for the electron-phonon interaction. The fits without the correction (dashed lines) are less satisfactory for all values of the spin-orbit scattering parameter λ_{so} than the fit with the correction (solid line).

cord with GLAG theory of type-II superconductivity. This is a nontrivial result for such complicated materials considering the idealized assumptions of the theory and that for these materials, unlike simple alloys, T_c, and the density of states $N(0)$ as well as the mean free path l_{tr} depend sensitively on the physical state of the material. Specifically we find that the temperature dependence of H_{c2} can be satisfactorily fitted using this theory (including both orbital and Pauli-paramagnetic pair breaking) and that electronic heat-capacity coefficient γ^* deduced from the data are in acceptable agreement with the values obtained directly from heat-capacity measurements. The cleaner samples exhibit some positive curvature near T_c that is not consistent with the simple GLAG theory. This curvature is similar to that observed in the elemental superconductors Nb and V (in the clean limit) which has been interpreted as resulting from anisotropy of the Fermi surface. The observed curvature is small in our samples, however, and it is not possible on the basis of the present data to establish whether or not it is an intrinsic effect.

Although our results conform to the GLAG theory, the picture of the high-field behavior of these superconductors that emerges regarding the effects of Pauli-paramagnetic limiting is different from that generally assumed. At the same time the systematic dependence of the superconducting and normal-state properties on residual resistivity measured in these experiments provides some new and useful information on A-15 compounds. We discuss each of these points and their possible broader implications in Sec. IV A.

A. Pauli limiting

As argued in Sec. III on simple theoretical grounds, the electron-phonon coupling corrections to the theory of Pauli limiting should be included for quantitative comparisons with experiment. Moreover it is found that to fit the data for Nb_3Sn and V_3Si with physically acceptable parameters it is necessary to include these corrections in the GLAG theory. Without their inclusion, well made Nb_3Sn is simply too clean to provide sufficient spin-orbit scattering to account for the observed lack of Pauli limiting. Inclusion of the electron-phonon corrections raises the Pauli-limiting field and thereby reduces the required spin-orbit scattering rate to a physically acceptable level (i.e., $\lambda_{so} \lesssim \lambda_{tr}$). In the case of V_3Si inclusion of these corrections leads to demonstrably better fits to the data. Insufficient spin-orbit scattering to account for the observed critical fields has been noted for the layered compounds as well[31] and may be a common feature of high-field ordered superconducting compounds. It is not clear, however, to what degree the electron-phonon-interaction enhancement of H_p provides a universal explanation of such effects. It must also be borne in mind that including electron-electron-interaction corrections will tend to reduce H_p and hence increase the required λ_{so}, possibly undermining the good fits obtained here. While we feel this is unlikely for Nb_3Sn and V_3Si, it cannot be ruled out absolutely. The combined effects of electron-phonon and electron-electron interactions on Pauli limiting needs further theoretical analysis.

In any event, since the major corrections to H_p from these sources arise from the different renormalizations of the densities of states governing the superconducting condensation energy and the normal-state spin susceptibility, and not from a strong coupling correction to the theory of superconductivity *per se*, they are never negligible for quantitative work. For example, the inclusion of the electron-phonon interaction corrections into the theory may help to resolve the discrepancy found by Meservey and Tedrow[32] in the spin-orbit scattering rates in-

ferred from critical-field measurements and tunneling measurements of the Zeeman splitting of the gap (for which we assume no corrections are necessary) in thin Al films. In a similar vein observation of the Zeeman splitting of the gap in V_3Si would directly confirm the picture presented in this paper. Such an experiment seems entirely feasible in light of recent advances in tunneling into thin films of V_3Si.[3]

B. Dependence of material properties on residual resistivity

The role of disorder (damage) in governing the properties of the A-15 superconductors has received considerable attention recently. Universal behavior of several physical properties as a function of ρ has been noted and even the possible existence of a universal defect underlying such behavior has been proposed.[7] The nature of the defects introduced into the A-15 materials under various treatments remains unresolved, although various points of view have been presented.[33]

The nature of the defects introduced into our samples by deposition at low substrate temperatures is unknown but site (antisite) disorder is perhaps the most obvious possibility. In any event the dependence of T_c and $(dH_{c2}/dT)_{T_c}$ on ρ observed with our samples (Fig. 4) is a good agreement with that observed previously in Nb_3Sn damaged with α-particle radiation, by Weismann *et al.*,[8] and in bulk V_3Si damaged by neutron irradiation by R. Viswanathan and R. Caton[10] and A. Guha *et al.*[34] In the latter case direct heat-capacity measurements were made which are in good agreement with the electronic heat-capacity coefficients determined on our films using critical-field measurements. Thus our data confirm universal behavior, but do not as yet help establish the nature of the defects present or their possible universality.

Finally we note that the range of critical fields possible with high-T_c Nb_3Sn is probably quite large as one goes from the clean to the dirty limit. Extrapolating the data of Fig. 4 to $\rho=0$, we find very clean Nb_3Sn should have $T_c \simeq 18.3$ K and $(dH_{c2}/dT)_{T_c} \simeq 16.2$ kOe/K leading to an $H_{c2}(0) \simeq 0.73(dH_{c2}/dT)_{T_c} \simeq 215$ kOe since we anticipate no appreciable Pauli limiting. By contrast in the dirty limit with $\rho = 35\,\Omega$ cm, T_c has dropped to only 16 K but $(dH_{c2}/dT)_{T_c}$ has risen to 26 kOe/K implying an $H_{c2}(0) \simeq 0.69(dH_{c2}/dT)_{T_c} T_c \simeq 290$ kOe as shown in Fig. 7. Thus critical fields up to almost 300 kOe appear possible using Nb_3Sn. Comparably high critical fields have also been observed by two of us[6] in the apparently nontransforming (i.e., cubic phase) portions of a single-crystal Nb_3Sn sample. The relation between this single-crystal data and the results reported here will require further investigation, including a more thorough characterization of the samples. V_3Si also would have a similar range of extrapolated critical fields but does not exhibit them in practice because of the presence of substantial Pauli limiting.

ACKNOWLEDGMENTS

We would like to thank R. E. Howard, R. H. Hammond, and T. H. Geballe for many useful discussions regarding the materials science and physics of the A-15 superconductors. One of us (TPO) is grateful for D. F. Moore's tutelage in both the experiments with and the properties of these A-15 thin films. Those of us from Stanford would like to thank the staff of the Francis Bitter National Laboratory for our pleasant visits there; and also S. T. Ruggiero for setting up the magnet facility at Stanford and helping us to understand the theory of type-II superconductors. The work at Stanford was supported by the U. S. DOE and the work at the Francis Bitter National Laboratory by the NSF. The support of these agencies is gratefully acknowledged.

APPENDIX

The strong-coupling equations used to evaluate the material parameters in Table II and III are outlined below.

Following Bergman and Rainer (see Ref. 13) we use the convention

$$Z(T) = \eta_Z(T) Z^{\mathrm{BCS}}(X^*) \tag{A1}$$

for any particular physical quantity [e.g., $H_{c2}(T)$], where Z^{BCS} is the weak-coupled BCS expression for the quantity Z, X^* stands for the normal-state parameters, the asterisk denotes that in evaluating Z^{BCS} one uses electron-phonon renormalized normal-state parameters, and $\eta_Z(T)$ is a factor reflecting the additional corrections due to the strong-coupled theory of superconductivity. Thus to use Eq. (A1) one requires expressions for $\eta_z(T)$ and Z^{BCS}.

1. Strong-coupling corrections—determination of η's, ω_0, and λ_{ep}

From the results of Refs. 18–20 we have

$$\eta_\Delta(0) = 1 + 5.3\left(\frac{T_c}{\omega_0}\right)^2 \ln\frac{\omega_0}{T_c}\ , \tag{A2}$$

$$\eta_{H_{c2}}(T_c) = 1 + \left(\frac{\pi T_c}{\omega_0}\right)^2 \left[0.6 \ln\frac{\omega_0}{T_c} - 0.26\right] , \quad \text{(A3)}$$

$$\eta_{H_c}(T_c) = 1 + \left(\frac{\pi T_c}{\omega_0}\right)^2 \left[1.1 \ln\frac{\omega_0}{T_c} + 0.14\right] , \quad \text{(A4)}$$

$$\eta_{\xi_{GL}}(T_c) = [\eta_{H_{c2}}(T_c)]^{-1/2} , \quad \text{(A5)}$$

$$\eta_{\lambda_{GL}}(T_c) = [\eta_{H_{c2}}(T_c)]^{1/2} \eta_{H_c}^{-1}(T_c) , \quad \text{(A6)}$$

$$\eta_{\kappa}(T_c) = \eta_{H_{c2}}(T_c) \eta_{H_c}^{-1}(T_c) , \quad \text{(A7)}$$

$$\eta_{H_c}(0) = 1 + 2.3 \left(\frac{T_c}{\omega_0}\right)^2 [\ln(\omega_0/T_c)] , \quad \text{(A8)}$$

where ω_0 is a characteristic (equivalent Einstein) frequency. In this paper ω_0 was determined using Eq. (A2) and the measured $2\Delta(0) k_B T_c = \eta_\Delta(0)$ (3.53). The other η's were then determined using this ω_0. To determine λ_{ep} one may use the T_c equation

$$T_c = 1.14\omega_0 \exp\left[-\frac{1 + 0.5\epsilon - 0.35\epsilon^2 + 0.8\epsilon\mu^*/(1+\lambda) + 0.4\mu^*\epsilon^2}{\epsilon - \mu^*/(1+\lambda) - 0.5\epsilon\mu^* - 1.5\mu^*\epsilon^2}\right] , \quad \text{(A9)}$$

where

$$\epsilon = \frac{\lambda}{1+\lambda}$$

and

$$\lambda = \lambda_{ep} .$$

2. BCS relationships — Z^{BCS}

Listed below are several BCS results for the material parameters of a superconductor in terms of T_c and normal-state quantities. This listing follows closely that of R. R. Hake[35] but is more complete and evaluates the numerical coefficients exactly. Note that there are only 4 *independent* parameters, for example, ρ, γ, T_c and the Fermi-surface area S. The parameters S_F and n are introduced only for convenience. They are related by the expression $S_F = 4\pi(3\pi^2 n)^{2/3}$ so that in fact the combination $n^{2/3}S/S_F$ that appears throughout is actually proportional to S.

The following symbols and units are used: low-temperature normal-state resistivity $\rho_{\Omega\,cm}$, where $\rho_{\Omega\,cm} = \frac{1}{9} \times 10^{-11} \rho_{cgs}$; the normal-state electronic specific-heat coefficient γ (erg cm^{-3} K^{-2}); the superconducting transition temperature T_c (K); the reduced temperature $t = T/T_c$, the jump in the specific heat at T_c, $c_S - c_N$; the conduction-electron density n (cm^{-3}), Fermi surface S (cm^{-2}), the Fermi surface of an electron gas of density n, S_F; the flux quantum ϕ_0(Oe cm^2); Planck's constant $\hbar$(erg sec); Boltzman's constant k_B(erg K^{-1}); the electronic charge e (esu); the velocity of light c (cm sec^{-1}); $\zeta(3) \approx 1.202$ and $e^\gamma \approx 1.781$.

1. Average Fermi velocity

$$\langle v_F \rangle = k_B^2 \hbar^{-1} (\pi^4/3)^{1/3} (n^{2/3}S/S_F) \gamma^{-1}$$
$$= 5.77 \times 10^{-5} (n^{2/3}S/S_F)\, \gamma^{-1} \text{cm sec}^{-1} .$$

2. Electronic mean free path

$$l_{tr} = 9 \times 10^{11}\, \hbar (3\pi^2)^{1/3} [e^2 \rho_{\Omega\,cm} (n^{2/3}S/S_F)]^{-1}$$
$$= 1.27 \times 10^4 [\rho_{\Omega\,cm} (n^{2/3}S/S_F)]^{-1} \text{cm} .$$

3. Density of states of one spin direction

$$N(0) = (2\pi^2 k_B^2/3)^{-1} \gamma$$
$$= 7.97 \times 10^{30} \gamma \text{ states cm}^{-3} \text{erg}^{-1} \text{spin}^{-1} .$$

4. BCS coherence length

$$\xi_0 = \hbar \langle v_F \rangle (\pi^2 e^{-\gamma} k_B T_c)^{-1}$$
$$= e^\gamma k_B (3\pi^2)^{-1/3} (n^{2/3}S/S_F) (\gamma T_c)^{-1}$$
$$= 7.95 \times 10^{-17} (n^{2/3}S/S_F) (\gamma T_c)^{-1} \text{cm} .$$

5. London penetration depth (0 K)

$$\lambda_{L0} = 3\, \hbar c \pi^{1/2} [2(3\pi^2)^{2/3} k_B e]^{-1} \gamma^{1/2} (n^{2/3}S/S_F)^{-1}$$
$$= 1.33 \times 10^8 \gamma^{1/2} (n^{2/3}S/S_F)^{-1} \text{cm} .$$

Gor'kov χ function

a. $\chi(\lambda_{tr}) = (1 + \lambda_{tr})^{-1} R(\lambda_{tr})$,

where $R(0) = 1$ and $R(\infty) = \pi^2 [7\zeta(3)]^{-1} = 1.17$ (See Ref. 9)

b. $\lambda_{tr} = \pi e^{-\gamma} \xi_0 (2 l_{tr})^{-1} = 0.882 \xi_0 / l_{tr}$
$$= k_B e^2 \rho_{\Omega\,cm} (3\pi^2)^{1/3} (n^{2/3}S/S_F)$$
$$\times (54 \times 10^{11} \pi\, \hbar \gamma T_c)^{-1}$$
$$= 5.51 \times 10^{-21} \rho_{\Omega\,cm} (n^{2/3}S/S_F) (\gamma T_c)^{-1} .$$

7. Ginzburg-Landau coherence length

a. *full value (λ_{tr} arbitrary).*

$$\xi_{GL} = \pi e^{-\gamma}[7\zeta(3)/48]^{1/2}\xi_0[\chi(\lambda_{tr})]^{1/2}(1-t)^{-1/2} = 0.739[\xi_0^{-2} + 0.882(\xi_0 l_{tr})^{-1}]^{-1/2}[R(\lambda_{tr})]^{1/2}(1-t)^{-1/2}$$
$$= \left\{144 T_c^2\gamma^2[7\zeta(3)k_B^2(3\pi^2)^{1/3}(n^{2/3}S/S_F)^2]^{-1} + 24e^2\rho_{\Omega\,cm}\gamma T_c[(63\times10^{11})\zeta(3)\pi k_B\hbar]^{-1}\right\}^{-1/2} R^{1/2}(\lambda_{tr})(1-t)^{-1/2}$$
$$= [2.90\times10^{32}T_c^2\gamma^2(n^{2/3}S/S_F)^{-2} + 1.60\times10^{12}\rho_{\Omega\,cm}\gamma T_c]^{-1/2}[R(\lambda_{tr})]^{1/2}(1-t)^{-1/2}\,\text{cm} \ .$$

b. *Clean limit ($\lambda_{tr} << 1$).*

$$\xi_{GL}^c = \pi e^{-\gamma}[7\zeta(3)/48]^{1/2}\xi_0(1-t)^{-1/2} = 0.739\xi_0(1-t)^{-1/2} = k_B(3\pi^2)^{2/3}[7\zeta(3)/3]^{1/2}(n^{2/3}S/S_F)(12\pi T_c\gamma)^{-1}$$
$$= 5.87\times10^{-17}(n^{2/3}S/S_F)(T_c\gamma)^{-1}\,\text{cm} \ .$$

c. *Dirty limit ($\lambda_{tr} >> 1$).*

$$\xi_{GL}^d = (\pi^3 e^{-\gamma}/24)^{1/2}(\xi_0 l_{tr})^{1/2}(1-t)^{-1/2} = 0.852(\xi_0 l_{tr})^{1/2}(1-t)^{-1/2} = (9\times10^{11}\pi^3 k_B\hbar)^{1/2}(24e^2\gamma\rho_{\Omega\,cm}T_c)^{-1/2}(1-t)^{-1/2}$$
$$= 8.57\times10^{-7}(\gamma\rho_{\Omega\,cm}T_c)^{-1/2}(1-t)^{-1/2}\,\text{cm} \ .$$

8. Ginzburg-Landau penetration depth

a. *Full value.*

$$\lambda_{GL} = 2^{-1/2}\lambda_{Lo}(1+\pi e^{-\gamma}\xi_0/2l_{tr})^{1/2}[R(\lambda_{tr})]^{-1/2}(1-t)^{-1/2} = 2^{-1/2}\lambda_{Lo}(1+0.882\xi_0/l_{tr})^{1/2}[R(\lambda_{tr})]^{-1/2}(1-t)^{-1/2}$$
$$= \left\{3c^2\hbar^2\gamma[8\pi e^2k_B^2(3\pi^2)^{1/3}(n^{2/3}S/S_F)^2]^{-1} + c^2\hbar\rho_{\Omega\,cm}(144\times10^{11}\pi^2k_BT_c)^{-1}\right\}^{1/2}[R(\lambda_{tr})]^{-1/2}(1-t)^{-1/2}$$
$$= [8.77\times10^{15}\gamma(n^{2/3}S/S_F)^{-2} + 4.83\times10^{-5}\rho_{\Omega\,cm}T_c^{-1}]^{1/2}[R(\lambda_{tr})]^{-1/2}(1-t)^{-1/2}\,\text{cm} \ .$$

b. *Clean limit.*

$$\lambda_{GL}^c = 2^{-1/2}\lambda_{Lo}(1-t)^{-1/2} = 3(2\pi)^{1/2}c\,\hbar\gamma^{1/2}[4ek_B(3\pi^2)^{2/3}(n^{2/3}S/S_F)]^{-1}(1-t)^{-1/2}$$
$$= 9.37\times10^7\gamma^{1/2}(n^{2/3}S/S_F)^{-1}(1-t)^{-1/2}\,\text{cm} \ .$$

c. *Dirty limit.*

$$\lambda_{GL}^d = 2^{-1/2}\lambda_{Lo}[7e^{-\gamma}\zeta(3)\xi_0/2\pi l_{tr}]^{1/2}(1-t)^{-1/2} = 2^{-1/2}\lambda_{Lo}(\xi_0/1.33l_{tr})^{1/2}(1-t)^{-1/2}$$
$$= [7c^2\hbar\zeta(3)\rho_{\Omega\,cm}]^{1/2}(144\times10^{11}\pi^4k_BT_c)^{1/2}(1-t)^{-1/2} = 6.42\times10^{-3}(\rho_{\Omega\,cm}/T_c)^{1/2}(1-t)^{-1/2}\,\text{cm} \ .$$

9. Ginzburg-Landau κ

a. *Full value.*

$$\kappa_{GL} = e^{\gamma}\lambda_{Lo}(\xi_0\pi)^{-1}[24/7\zeta(3)]^{1/2}(1+\pi e^{-\gamma}\xi_0/2l_{tr})[R(\lambda_{tr})]^{-1} = 0.957\lambda_{Lo}\xi_0^{-1}(1+.882\xi_0/l_{tr})[R(\lambda_{tr})]^{-1}$$
$$= \left\{3c\,\hbar T_c\gamma^{3/2}[6/7\pi\zeta(3)]^{1/2}[ek_B^2(3\pi^2)^{1/3}(n^{2/3}S/S_F)^2]^{-1} + ce\gamma^{1/2}\rho_{\Omega\,cm}[6/7\pi^3\zeta(3)]^{1/2}(18\times10^{11}k_B)^{-1}\right\}[R(\lambda_{tr})]^{-1}$$
$$= [1.60\times10^{24}T_c\gamma^{3/2}(n^{2/3}S/S_F)^{-2} + 8.78\times10^3\gamma^{1/2}\rho_{\Omega\,cm}][R(\lambda_{tr})]^{-1} \ .$$

b. *Clean limit.*

$$\kappa_{GL}^c = e^{\gamma}\lambda_{Lo}(\xi_0\pi)^{-1}[24/7\zeta(3)]^{1/2} = 0.957\lambda_{Lo}/\xi_0 = 3c\,\hbar T_c\gamma^{3/2}[6/7\pi\zeta(3)]^{1/2}[ek_B^2(3\pi^2)^{1/3}(n^{2/3}S/S_F)^2]^{-1}$$
$$= 1.60\times10^{24}T_c\gamma^{3/2}(n^{2/3}S/S_F)^2 \ .$$

c. *Dirty limit.*

$$\kappa_{GL}^d = \lambda_{Lo}l_{tr}^{-1}[42\zeta(3)/\pi^4]^{1/2} = 0.720\lambda_{Lo}/l_{tr} = ce\gamma^{1/2}\rho_{\Omega\,cm}[42\zeta(3)/\pi^7]^{1/2}(18\times10^{11}k_B)^{-1} = 7.49\times10^3\gamma^{1/2}\rho_{\Omega\,cm} \ .$$

10. Thermodynamic critical field

$$H_c = 4[3\pi/7\zeta(3)]^{1/2}\gamma^{1/2}T_c(1-t) = 4.23\gamma^{1/2}T_c(1-t)\text{Oe} \ .$$

11. Slope of thermodynamic critical field

$$-(dH_c/dT)_{T_c} = [4\pi(c_s - c_n)/T_c]^{1/2} = 4[3\pi/7\zeta(3)]^{1/2}\gamma^{1/2} = 4.23\gamma^{1/2}\text{Oe K}^{-1} \ .$$

12. Slope of upper critical field

a. *Full value.*

$$-(dH_{c2}/dT)_{T_c} = \left\{24\pi^2 \hbar c \gamma^2 T_c[7\zeta(3)k_B^2 e(\pi^4/3)^{2/3}(n^{2/3}S/S_F)^2]^{-1} + 12ec\gamma\rho_{\Omega\,\text{cm}}[63\times10^{11}\pi k_B\zeta(3)]^{-1}\right\}[R(\lambda_{\text{tr}})]^{-1}$$

$$= [9.55\times10^{24}\gamma^2 T_c(n^{2/3}S/S_F)^{-2} + 5.26\times10^4\gamma\rho_{\Omega\,\text{cm}}][R(\lambda_{\text{tr}})]^{-1}\text{Oe K}^{-1} \ .$$

b. *Clean limit.*

$$-(dH_{c2}/dT)^{c}_{T_c} = 24\pi^2 \hbar c \gamma^2 T_c[7\zeta(3)k_B^2 e(\pi^4/3)^{2/3}(n^{2/3}S/S_F)^2]^{-1} = 9.55\times10^{24}\gamma^2 T_c(n^{2/3}S/S_F)^2\text{Oe K}^{-1} \ .$$

c. *Dirty limit.*

$$-(dH_{c2}/dT)^{d}_{T_c} = 24e^{\gamma}\hbar c(\pi^3\xi_0 l_{\text{tr}}T_c)^{-1} = 12ec\gamma\rho_{\Omega\,\text{cm}}(9\times10^{11}\pi^3 k_B)^{-1} = 4.48\times10^4\gamma\rho_{\Omega\,\text{cm}}\text{Oe K}^{-1} \ .$$

13. Lower critical field

$$H_{c1} = H_c \ln\kappa[(2)^{1/2}\kappa]^{-1} \ .$$

---

[1] R. H. Hammond, IEEE Trans. Mag. MAG- 11, 201 (1975); R. H. Hammond, J. Vac. Sci. Technol. 15, 382 (1978).

[2] B. E. Jacobson, R. H. Hammond, T. H. Geballe, and J. R. Salem, J. Less Common Metals (to be published).

[3] D. F. Moore, J. M. Rowell, and M. R. Beasley, Solid State Commun. 20, 305 (1976); D. F. Moore, thesis (Stanford University, 1978), (Ginzton Laboratory Report No. 2788); D. F. Moore, M. R. Beasley, and J. M. Rowell submitted to LT 15 Conference, Grenoble, France (unpublished).

[4] L. J. van der Pauw, Philips Res. Rep. 13, 1 (1958).

[5] A. L. Fetter and P. C. Hohenberg, in *Superconductivity*, edited by R. E. Parks (Marcel Dekker, New York, 1969), Vol. II, p. 866.

[6] S. Foner and E. J. McNiff, Jr., Phys. Lett. A 58, 318 (1976); S. Foner and E. J. McNiff, Jr., Appl. Phys. Lett. 32, 122 (1978).

[7] L. R. Testardi, J. M. Poate, and H. J. Levinstein, Phys. Rev. B 15, 2570 (1977).

[8] H. Wiesmann, M. Gurvitch, A. K. Ghosh, H. Lutz, O. F. Kammerer, and M. Strongin, Phys. Rev. B 17, 122 (1978).

[9] N. R. Werthamer, in Ref. 5, pg. 321.

[10] R. Viswanathan and R. Caton, Phys. Rev. B 18, 15 (1978).

[11] G. Grimvall, Phys. Scr. 14, 63 (1976).

[12] P. B. Allen and R. C. Dynes, Phys. Rev. B 12, 905 (1975).

[13] D. Rainer and G. Bergmann, J. Low Temp. Phys. 14, 501 (1974).

[14] D. Rainer, G. Bergmann, and U. Eckhardt, Phys. Rev. B 8, 5324 (1973).

[15] G. Eilenberger and V. Ambegaokar, Phys. Rev. 158, 322 (1967).

[16] K. D. Usadel, Phys. Rev. B 2, 135 (1970).

[17] N. R. Werthamer and W. L. McMillan, Phys. Rev. 158, 415 (1967).

[18] N. F. Masharov, Sov. Phys. Solid State 16, 1524 (1975).

[19] V. Z. Kresin and V. P. Parkhomenko, in Ref. 18, p. 2180.

[20] B. T. Geilikman, V. Z. Kresin, and N. F. Masharov, J. Low Temp. Phys. 18, 241 (1975).

[21] A. Junod, J. Muller, H. Rietschel, and E. Schneider, J. Phys. Chem. Solids 39, 317 (1978).

[22] L. J. Vieland and A. W. Wicklund, Phys. Rev. 166, 424 (1968).

[23] The parameters S_F and n are useful only in estimating S and are not necessary; this is manifest if one notes that $S_F = 4\pi(3\pi^2 n)^{2/3}$ so that the factor $n^{2/3}S/S_F$ that appears throughout is proportional only to S. In this paper, we have conveniently chosen n as the number of valence electrons per unit volume; $n = 2.59\times10^{23}$ valence electrons/cm^3 for Nb_3Sn and $n = 3.67\times10^{23}$ valence electrons/cm^3 for V_3Si.

[24] R. E. Howard, D. A. Rudman, and M. R. Beasley, Appl. Phys. Lett. 33, 671 (1978). The high-κ A-15 superconductors have $\lambda(T) > (\xi_0^{-1} + l_{\text{tr}}^{-1})^{-1}$ so that the elec-

tromagnetic field acts locally. In addition for a dirty superconductor ($\lambda_{tr} >> 1$), P. D. Scholten *et al.* [Physical Review B 16, 1068 (1977)] have found

$$\lambda(T) = \lambda^{BCS}(x^*)[I(T)|^{BCS}/I(T)]^{1/2}$$
$$= \lambda^{BCS}(x^*) n_\lambda(T) \ .$$

In the weak-coupled BCS limit,
$\lambda^{BCS}(T=0) = 2^{1/2}\lambda_{GL}^{BCS}(0)(1.33)^{1/2}$ where
$\lambda_{GL}(T \approx T_c) = \lambda_{GL}(0)(1 - T/T_c)^{-1/2}$. Therefore, in the local and dirty limits

$$\lambda(T=0) = 2^{1/2}\lambda_{GL}^{BCS}(0,*)(1.33)^{1/2}\eta_\lambda(0)$$
$$= 2^{1/2}\lambda_{GL}(0)(1.33)^{1/2}\eta_\lambda(0)/\eta_\lambda(T_c) \ .$$

For arbitrary mean free path we have assumed the above form for $\lambda(T=0)$ with $(1.33)^{1/2}$ replaced by the ratio in Table I of P. B. Miller [Phys. Rev., 113, 1209 (1959)]. We have assumed $\eta_\lambda(0) = [\eta_\Delta(0)]^{-1/2}$ since $\eta_\lambda(T_c) = [\eta_\Delta(T_c)]^{-1/2}$.

[25]E. Helfand and N. R. Werthamer, Phys. Rev. 147, 288 (1966).

[26]N. R. Werthamer, E. Helfand, and P. C. Hohenberg, Phys. Rev. 147, 295 (1966).

[27]K. Maki, Phys. Rev. 148, 362 (1966).

[28]A. M. Clogston, Phys. Rev. Lett. 9, 266 (1962).

[29]For simple metals with no electron-phonon interaction, the electron-electron interaction increases the Pauli spin susceptibility χ_p to $\chi_p = \chi_p^b/(1-I)$, where I is the Stoner factor, and would consequently decrease the Pauli limiting field H_p. If the electron-phonon interactions are also included, the ratio of the specific-heat density of states to the Pauli spin susceptibility is no longer straightforward, but certainly the effect of electron-electron interaction will continue to be to decrease H_p.

[30]For bulk type-II superconductors in the dirty limit, $H_{c2}(t)$ is an implicit function of

$$\ln t = \psi\left(\frac{1}{2}\right) - \frac{1}{2}\left(1 + \frac{\lambda_{so}/4}{X}\right)\psi\left(\frac{1}{2} + \frac{Y + \lambda_{so}/4 - X}{t}\right)$$
$$- \frac{1}{2}\left(1 - \frac{\lambda_{so}/4}{X}\right)\psi\left(\frac{1}{2} + \frac{Y + \lambda_{so}/4 + X}{t}\right) \ ,$$

where ψ is the digamma function,

$$Y = \frac{2h}{\pi^2}, \quad t = T/T_c$$
$$h = H_{c2}(T)/\left[\frac{dH_{c2}}{dT}|_{T_c} T_c\right]$$
$$X = [(\lambda_{so}/4)^2 - 4h^2\alpha^2/\pi^4]^{1/2}$$
$$\alpha = \frac{2^{1/2}\pi^2}{8e^\gamma} \frac{-(dH_{c2}/dT|_{T_c})T_c}{H_p(0)}$$

and we have taken

$$H_{p(0)} = \frac{\pi}{2^{1/2}e^\gamma}\frac{k_B}{\mu_B} T_c[(1+\lambda_{ep})^{1/2}\eta_{H_c}(0)] \ .$$

[31]A. Luther, M. R. Beasley and R. A. Klemm, Proceedings of the Nobel Symposium XXIV, Stockholm, 1973 (unpublished); and D. Prober, R. E. Schwall, and M. R. Beasley (unpublished).

[32]Compare results obtained for Al via critical-field measurements [P. M. Tedrow and R. Meservey, Phys. Rev. B 8, 5098 (1973)] and via tunneling [R. Meservey, P. M. Tedrow, and R. C. Bruno, Phys. Rev. B 11, 4224 (1975)].

[33]See for example R. Viswanathan, R. Caton, and C. S. Pande, Phys. Rev. Lett. 41, 906 (1978) and references cited therein.

[34]A. Guha, M. P. Sarachik, F. W. Smith, L. R. Testardi, Phys. Rev. 18, 9 (1978).

[35]R. R. Hake, Phys. Rev. 158, 356 (1966).